Desalination and Water Treatment
www.deswater.com
doi: 10.5004/dwt.2018.23032

132 (2018) 52–62
November

Heat and mass transfer characteristics in vacuum membrane distillation for water desalination

Elham El-Zanati*, Maaly Khedr, Ayman El-Gendi, Heba Abdallah, Eman Farg, Esraa Taha

Chemical Engineering and Pilot Plant Department, Engineering Research Division, National Research Centre, 33El-Bohouth St. (Former El Tahrir St.), Dokki, Giza, Egypt, P.O. box 1262. Affiliation ID: 60014618, Tel. 202 33335494, Fax 202 33370931, email: eelzanati@gmail.com (E. El-Zanati), maalykheder@yahoo.com (M. Khedr), aymantaha2010@yahoo.com (A. El-Gendi), heba_nasr94@yahoo.com (H. Abdallah), demfarg@gmail.com (E. Farg), esraa.che13@gmail.com (E. Taha)

Received 8 February 2018; Accepted 27 August 2018

ABSTRACT

The vacuum membrane distillation (VMD) is applied in desalination. The simultaneous heat and mass transfer and the operating condition are studied. The experiments were carried out on a laboratory VMD unit, using a pre-prepared flat sheet membrane. Feed solutions used were fresh and saline water ranged from 3000 to 40,000 ppm. The operating parameters studied was feed temperature (298–368K), absolute pressure at downstream of the membrane (80,000–20,000 Pa), feed velocity (0.001–0.004 ms^{-1}). The permeability of the prepared membrane is measured by two methods; the results showed the feasibility and applicability of these methods. The operating conditions and membrane characteristics are proved crucial factors influencing the permeation through the membrane. The experimental data were used to estimate the individual liquid film transfer coefficients. The operating condition dependence is demonstrated. The results are expressed in an equation for each coefficient; temperature (T), pressure (P), feed velocity (v) and concentration (C). Also, the obtained empirical correlations at the liquid-vapor interface are expressed as a function in T, P, v, and C. Moreover, an empirical correlation for the Sherwood number is formulated. The developed empirical correlations are proved to be capable in predicting the VMD transport coefficients, and it may play a key in the process design and performance.

Keywords: Vacuum membrane distillation; Heat transfer; Mass transfer; Permeability; Desalination

1. Introduction

Membrane distillation (MD) is a concurrent combination of thermal distillation and membrane separation processes. It offers various advantages in comparison to the traditional distillation and pressure-driven membrane processes [1,2]. The merits of MD compared to other more popular separation processes stem from [3]:

- A complete rejection of salt molecules (100% "theoretical" rejection), macromolecules and other non-volatile compounds.
- Lower operating temperatures than conventional distillation.
- Lower operating pressures than conventional pressure-driven membrane separation processes.
- MD can potentially minimize brine volume at lower energy expenditure and with less complexity.
- Less demanding membrane mechanical property requirements, and
- Reduced vapor spaces compared to conventional distillation processes.

Recently, vacuum membrane distillation (VMD) one of the different MD configurations has received much attention as a promising and cost-effective separation process in water desalination. It is a separation process, in which, the water vapor diffuses through a porous hydrophobic membrane barrier. The process counts on motivating a pressure/temperature gradient across the membrane; the

*Corresponding author.

feed side is that in direct contact with the aqueous solution, and the permeate side, which is continuously kept under vacuum to generate a driving force for transmembrane flux. Moreover, permeate pressure values must be smaller than the equilibrium vapor pressure of the feed to avoid condensation, the water vapor removed is to be condensed in a separate condenser.

The presence of a reasonably high vacuum on the other side of the membrane in VMD considerably reduces the extent of conductive heat loss from the hot feed. The pores in the hydrophobic porous membrane surface exposed to hot feed are not supposed to be wet [4].

Many investigators have noted the importance of the heat transfer coefficient in different forms of MD, including VMD [4]. VMD has been actively explored to remove vapors from aqueous solutions. An additional benefit of VMD studies is the possibility of obtaining a characterization of the hot feed side heat transfer coefficient [5]. Selection of the proper membrane is a function of the membrane characteristics, such as porosity, contact angle, permeability, etc. Therefore, a research program was undertaken by the authors to prepare a new flat sheet hydrophobic porous membrane formulated of a blend of polyethersulfone/tetraethylorthosilicate (PES/TEOS). The developed membrane was prepared by phase inversion via immersion precipitation method. A dope solution comprises PES, N-methylpyrrolidone, polyvinylpyrrolidone (pore former) and tetraethylorthosilicate (raising the membrane hydrophobicity), the solution was, then, stirred at 400 rpm, 4 h at around 25 ± 2°C. The obtained homogeneous polymeric solution was kept several hours to remove the air bubbles. The solution was sprinkled, cast on a glass plate, and then moved to the non-solvent coagulation bath (water). The developed membrane was characterized using scan electron microscopy (SEM), its contact angle was measured. The membrane was, then, tested by VMD laboratory unit using NaCl solutions [6]. In the present paper, the influence of operating conditions on the mass and heat transfer coefficients, and consequently the effect on VMD performance, is studied.

2. Theory

2.1. Membrane permeability

The mass transfer occurs by diffusion of the vapors across the membrane; where the Knudsen diffusion is prevailing. It suggests a linear relationship between the water flux, J_{H_2O}, and the water vapor pressure difference between the membrane side surfaces, viz Eq. (1) [5]:

$$J_{H_2O} = K_K * \Delta P_{H_2O} = K_K * \left(P_m^* - P_p\right) \quad (1)$$

where J_{H_2O}, is the molar flux of water, ΔP_{H_2O} is the difference in partial pressure of water vapor on both sides of the membrane; P_m* is the vapor pressure of pure water at equilibrium conditions; P_p is the vapor pressure of water in the permeate side, which is equal to vacuum pressure as the permeate is only composed of water, and K_K is a membrane coefficient. Remarkably, the K_K parameter does not associate to the permeate, but it depends only upon the membrane properties and slightly on temperature ($T_m^{-0.5}$).

Eq. (2) expresses the membrane coefficient K_K [5]:

$$K_K = \frac{2\varepsilon r}{3\chi\delta RT_m}\sqrt{\frac{8RT_m}{\pi M_{H_2O}}} = \frac{K_m}{\sqrt{M_{H_2O}}} \quad (2)$$

where ε is the membrane porosity; r is the pore size; χ is the tortuosity factor; δ is the membrane thickness; R is the universal gas constant, M_{H_2O} is the molar mass of water, K_m is the Knudsen permeability and T_m is the temperature at the membrane surface. Owing to the applied vacuum pressure; the boundary layer in the permeate side may be neglected, which implies a reduction in the heat conduction through the membrane in VMD [5].

The variation of trans-membrane partial pressure difference ΔP_{H_2O} in VMD, was related to varying bulk temperature at a fixed initial permeate pressure. The different value of the permeate flux, J_{H_2O}, can be achieved by matching to the different value at the bulk temperature. The permeate flux can be calculated from Eq. (3) [5].

$$J_{H_2O} = \frac{K_m(T)}{\sqrt{M_{H_2O}}}\Delta P_{H_2O} = \frac{K_m\left(T_{ref}\right)}{\sqrt{M_{H_2O}}}\sqrt{\frac{T_{H_2O}}{T}}\Delta P_{H_2O} \quad (3)$$

According to Eq. (3), determination of the membrane permeability, K_m, is accomplished by changing of transmembrane partial pressure while recording the corresponding change in the permeate flux. This can be attained by either varying the applied vacuum pressure at a constant bulk temperature (pressure variation method) or vice-versa (temperature variation method). The relationship between the two factors; the vapor flux $\left(J_{H_2O}\right)$ and either the pressure gradient (ΔP_{H_2O}) or this term $\left(\sqrt{\frac{T_{ref}}{T}}\Delta P_{H_2O}\right)$ offers a straight line with its slope α, and gives directly the value of Knudsen permeability, K_m at reference temperature T_{ref}= 20°C (room temperature).

2.2. Heat and mass transfer coefficients

Membrane distillation (MD) is a non-isothermal process. The heat transfer mechanism comprises of the latent heat (phase change) occurring during the process and conduction through the membrane. Fig. 1 represents a diagram of the heat transfer resistances involved.

In VMD configuration, a pump is used to create a vacuum in the permeate side where condensation takes place outside the membrane module. Thus, the following steps characterize VMD: vaporization of the more volatile component in the liquid mixture at the liquid-vapor (l-v) interface and diffusion of the vapor through the membrane according to Knudsen mechanism. The heat transfer to the

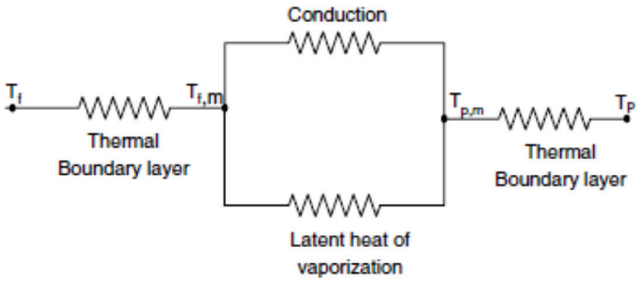

Fig. 1. Heat transfer resistances in the MD system.

liquid interface/membrane must be considered to determine the required energy for feed evaporation. Consequently, the relevant resistances determining the process performance are associated with both heat and mass transfer through the liquid interface as well as mass transfer through the membrane.

Generally, referring to the above resistances (Fig. 1), the heat transfer mechanism can be expressed by Eqs. (4)–(9) [1,5]:

Heat transfer by convection in the feed boundary layer:

$$Q_f = h_f (T_f - T_{fm}) \tag{4}$$

Heat transfer through the membrane layer:

$$Q_m = h_m (T_{fm} - T_{pm}) + J\Delta H_v \tag{5}$$

Heat transfer through the permeate boundary layer:

$$Q_p = h_p (T_{pm} - T_p) \tag{6}$$

At steady state:

$$Q = Q_f = Q_m = Q_p \tag{7}$$

Hence, the overall heat transfer flux through the membrane is given by:

$$Q = U(T_f - T_p) \tag{8}$$

where h is heat transfer coefficient (f feed boundary layer, m membrane layer, and p permeate boundary layer), U is the overall heat transfer coefficient, T is temperature (T_f feed temperature, T_{fm} temperature on membrane surface on the feed side, T_{pm} temperature on membrane permeate side and T_p temperature on permeate side).

The heat transfer by conduction through the membrane layer is expressed as follows:

$$h_m = \left(C_m \frac{dP}{dT} \right) \Delta H_v + \frac{k_m}{\delta} \tag{9}$$

where K_m is the thermal conductivity, δ is the membrane thickness and ΔHv is the heat of vaporization [7–9].

Lawson and Lloyd [3] pointed out that the ($T_{fm} - T_{pm}$) is about 0.02–0.1°C, at low flux, it does not exceed 0.5°C, at high flux, however, heat transfer by conduction and convection through the membrane can be ignored [1,10,11].

Since the VMD process is a simultaneous heat and mass transfer phenomena; the mass and heat transfer coefficients are related to Reynolds analogy [7,12].

$$\frac{h_f}{k_f} = \rho C_p \left[\frac{Sc}{Pr} \right]^{2/3} \tag{10}$$

where K_f is the mass transfer coefficient of feed boundary layer, ρ is the density of water, C_p is the specific heat, and S_c is Schmitt number $\left[Sc = \frac{\mu}{\rho D} \right]$, and Pr is Prandtl number $\left[\Pr = \frac{C_p}{k} \mu \right]$.

The Dittus-Boelter empirical correlation used to estimate the heat transfer coefficient of the boundary layers, and consequently, the mass transfer coefficient can be calculated in terms of Nusselt number [1,13]:

$$Nu = constant \cdot Re^a \cdot Pr^b \tag{11}$$

where: for laminar flow $Re < 2100$ [9], Nu is expressed as:

$$Nu = 1.86 \left(\frac{Re \cdot Pr \cdot d_h}{L} \right)^{1/3} \tag{12}$$

Reynolds number can be calculated using Eq. (13).

$$Re = \frac{vd\rho}{\mu} \tag{13}$$

where v, d, ρ, μ and C_p are fluid velocity, density, viscosity, and heat capacity, respectively.

The Sherwood number, Sh, is called the mass transfer Nusselt number, and is defined as follows:

$$Sh = \frac{k_f \cdot d}{D} \tag{14}$$

3. Experimental procedure

The VMD experimental set-up in laboratory scale was designed in our previous work [6]. The apparatus components are shown in Fig. 2.

In this study, the experiments were carried out by the use of the newly prepared PES/TEOC hydrophobic flat membrane, located in a circular holder of 0.142 m diameter. The membrane properties are depicted in Table 1.

The experiments, were conducted at different operating parameters, namely: absolute pressure of downstream ranging from 800 to 200 mbar, i.e. 20–80% vacuum (low to high) vacuum pressure, which is equivalent to 80000–20000 Pa absolute pressure, feed temperature (298–368K), feed flow rate (0.000008–0.000028 m^3s^{-1}). Feed solutions were pure water for membrane permeability determination,

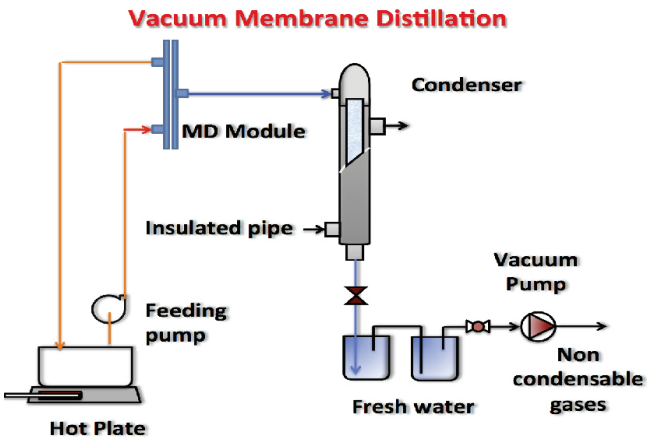

Fig. 2. Schematic diagram of VMD experimental laboratory set-up.

Table 1
The physical properties of the used membrane

Parameter	Value
Thermal conductivity, W m^{-1} K^{-1}	0.05
Pore diameter, µm	0.2
Thickness, µm	100
Porosity%	70
Tortuosity	1.43
Contact angle, °	125
Flux, l/m^2h	25–120
Salt rejection %	97–99

and synthetic NaCl solutions at different concentration (3000–40000 ppm), simulating brackish water and seawater. For each considered parameter, the permeate flux was recorded until a steady value is observed. The concentrate concentration was determined by evaluating the thermal conductivity and TDS.

4. Results and discussions

4.1. Pure water experiments

4.1.1. Dependence of permeate flow rate on temperature

Fig. 3 demonstrates the effect of feed temperature on permeate flux at 20000 Pa absolute pressure (equivalent to 20% vacuum), 0.000014 m^3 s^{-1} flow rate and feed velocity 0.00177 ms^{-1}. As observed, increasing the feed temperature leads to a significant increase in permeate flux (up to110 $kg{\cdot}m^{-2}$ h^{-1} at 368K feed temperature after 1800 s operating time), which is mainly due to higher heat flux through the liquid stream required for the interfacial water evaporation. This performance is explained by Antoine equation relating the water vapor pressure at the liquid/membrane interface with the temperature [14]. It is, also, noticed that the permeate flux values were relatively constant with process time for different temperatures up

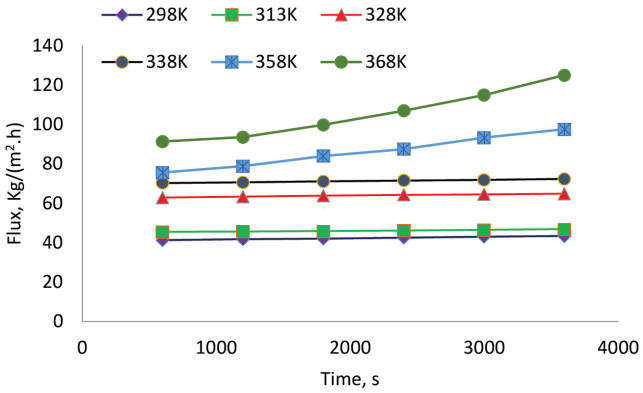

Fig. 3. Effect of feed temperature variation on permeate flux for pure water feed.

to 338K. However, increasing the temperatures (358 and 368K) increases the permeate flux slightly over time. This behavior is probably attributed to the higher temperature sensitivity of the membrane which might affect the membrane morphology by changing some of its geometric characteristics. For instance, a higher temperature may lead by time to minor membrane compaction followed by enhanced mass transport owing to shorter vapor diffusion paths. Moreover, these temperature conditions may exhibit an increase in membrane pore size during the first 1800 s of the process, and consequently, the permeate flux is slowly enhanced.

4.1.2. Dependence of permeate flow rate on vacuum pressure

Fig. 4 illustrates the effect of vacuum pressure on permeate flux of pure water. The experiments were carried out at a fixed flow rate (0.000014 m^3 s^{-1}), feed velocity 0.00177 m s^{-1} and temperature (338K). The results indicate that the highest flux was 72.3 $kg{\cdot}m^{-2}$ h^{-1} at 20000 Pa absolute pressure. The observed flux increases with increasing the applied vacuum pressure, it is attributed to the increase in the transmembrane water vapor pressure difference created because of a higher-pressure difference. This difference represents the driving force for mass transfer across the membrane. As expected, the flux was constant during process time at different operating vacuum pressures, due to static conditions used at each pressure value.

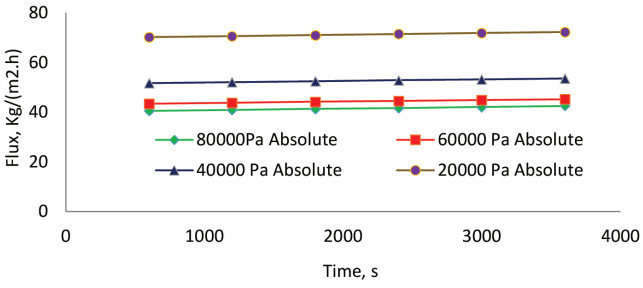

Fig. 4. Effect of absolute pressure on membrane flux during process time.

4.1.3. Determination of membrane permeability

a. Pressure variation method

The variation of partial pressure difference at different feed temperatures is plotted versus permeate molar flux as shown in Fig. 5. The line correlating J and ΔPv obtained by linear regression of the experimental results, gives J = 1E – 7ΔPv, (Fig. 5), the negative term (–0.0051) can be neglected, because it is an experimental error.

The slope of the straight line is the membrane coefficient (K_K), depending on permeate flux dimensions. The Knudsen permeability is then calculated from Eq. (2) giving the value of 4.24E-07 (s mol$^{1/2}$ m^{-1} kg$^{-1/2}$).

b. Temperature variation method

Furthermore, referring to Eq. (3), the permeate flux was plotted versus the partial pressure difference multiplied by the root of the ratio of temperature (reference temperature to feed temperature) . The slope of the obtained straight line gives the value of the Knudsen permeability from Eq. (3), as shown in Fig. 6, it equals to 3.82E–07 (s mol$^{1/2}$ m^{-1} kg$^{-1/2}$).

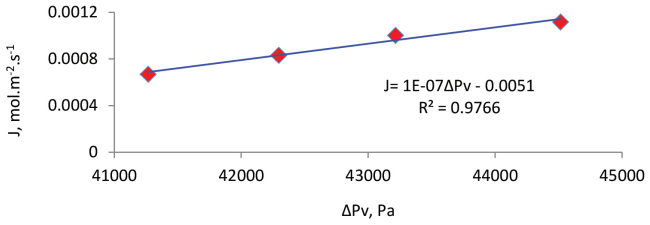

Fig. 5. Permeate flux vs partial pressure difference.

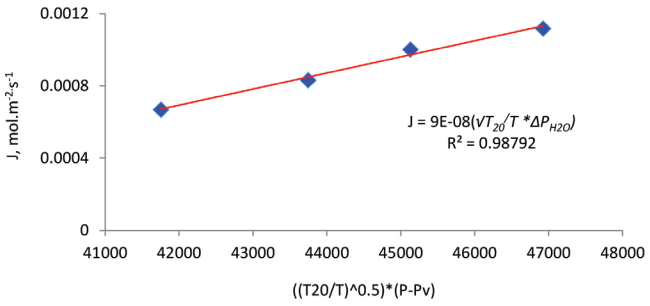

Fig. 6. Permeate flux measurement using temperature variation for Knudsen permeability determination.

The merely equal values of Knudsen permeability of the pre-prepared membrane (PES/TEOS blend), assured that both methods (pressure variation or temperature variation) are applicable [5].

4.1.4. Determination of heat and mass transfer coefficients

a. Effect of feed temperature

As mentioned above, the feed temperature has a robust influence on the permeate flux, where it increases when the temperature of the feed rises [15].

The heat transfer across the boundary layers, on both sides of the membrane, is often considered the rate-limiting step for mass transfer, owing to a large quantity of heat required and supplied to the vapor-liquid interface for liquid evaporation [1]. The values of heat transfer of water feed boundary layer were calculated using Eq. (4). Fig. 7 displays a plot of the heat transfer coefficient over 302 K to 332 K temperature range at 0.000014 m^3 s^{-1} feed flow rate (0.00177 ms^{-1}) and 20000 Pa absolute pressure.

As the heat transfer coefficient increases, the temperature at the membrane surface approaches to the bulk temperature and the vapor pressure driving force is increased [11,16]. Table 2 illustrates the heat transfer parameters at different temperatures, which indicates increasing heat flux and corresponding overall heat transfer coefficient by temperature increase.

As T_f increases, the temperature polarization factor ($\theta = (T_f - T_{fm})/(T_f - T_V)$) approaches zero since the feed temperature at the membrane surface approaches the bulk feed temperature. Subsequently, the heat transfer resistance in the feed boundary layer became negligible (as confirmed by the increase in U values), thus, the mass transfer across the membrane is the rate-limiting step in the process, and it is increased by increasing the feed temperature. This

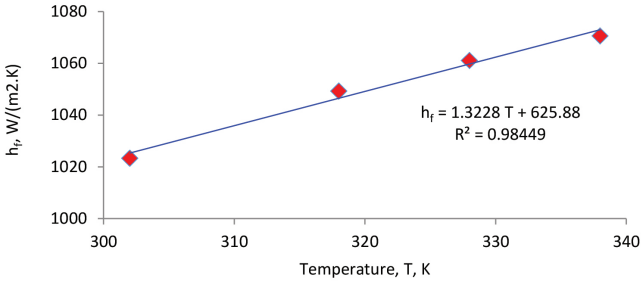

Fig. 7. Heat transfer coefficient in the feed boundary layer vs. feed temperature at feed flow rate 0.000014 m^3 s^{-1} (0.0018 m s^{-1}) and 20000 Pa absolute pressure.

Table 2
Heat transfer variables and parameters of VMD system at different temperatures

T_f, K	Q, W/m^2	U, W/m^{2}K	Re, ρuL/μ	Pr, cpμ/λ	Nu, h_fL/k	Sc, μ/ρD	Sh, k_fL/D
302	4093	1023	307	5.58	238.23	0.041	46.27
318	9444	1049	417	3.92	234.66	0.030	46.28
328	18041	1061	491	3.26	232.91	0.026	46.28
338	26766	1071	567	2.77	231.40	0.022	46.28

performance is sustained by the observed increase of Re, a decrease of Pr and Sc, as a consequence of water physical properties dependency on temperature.

Additionally, the mass transfer coefficient, k_f, was calculated by using the heat-mass transfer analogy at different temperatures and illustrated in Fig. 8.

The following simplified equations of heat and mass transfer are correlated using linear regression [7]:

$$h_f = 1.3228\ T_f + 625.88 \quad (15)$$

$$k_f = (5E-8)\ T_f + 0.0065 \quad (16)$$

b. Effect of feed velocity

The effect of feed velocity variation on the Re number and the heat transfer dependency expressed in terms of *Nu* number was investigated at fixed vacuum pressure 20000 Pa absolute pressure and 338K feed temperature. The feed velocity was varied between 0.0010 to 0.0036 ms^{-1}, it is included in the laminar regime where *Re* < 2100 (Eq. (12)) [10,12,17]. Fig. 9 illustrates the effect of feed velocity on *Re* and *Nu* numbers. As expected, working at a high feed velocity minimizes the boundary layer resistance and maximizes the convective heat transfer coefficient [18,19], and thus reduce the temperature polarization [17].

The relations between heat and mass transfer coefficients and the feed velocity, *v*, can be correlated according to Figs. 10 and 11 with following simplified equations respectively:

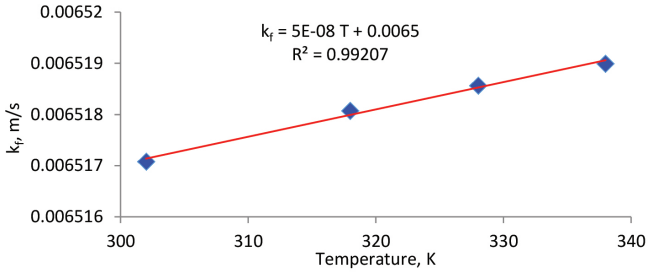

Fig. 8. Dependence of mass transfer coefficient in the feed boundary layer on feed temperature at feed flow rate 0.000014 $m^3 s^{-1}$ (0.0018 m s^{-1}) and 20000 Pa absolute pressure.

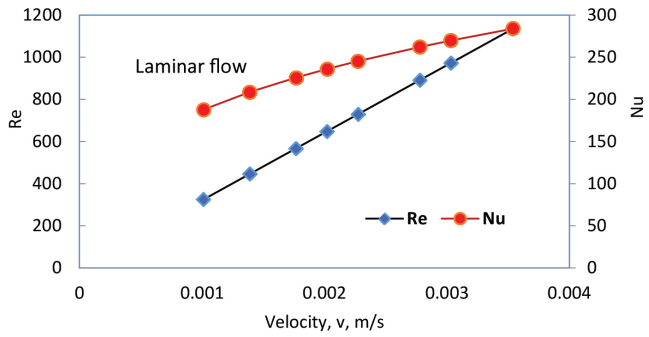

Fig. 9. Effect of increasing feed velocity on Reynolds and Nusselt numbers.

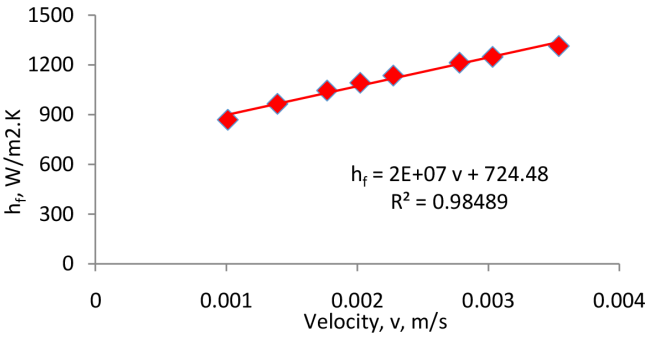

Fig. 10. The relation between the heat transfer coefficient and feed velocity at feed temperature 338 K and 20000 Pa absolute pressure.

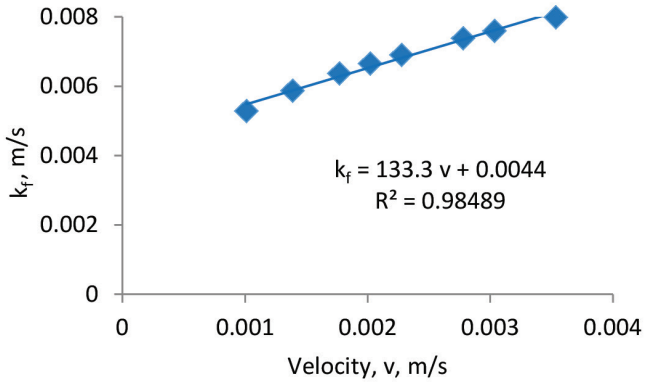

Fig. 11. The relation between the mass transfer coefficient and feed velocity at feed temperature 338 K and 20000 Pa absolute pressure.

$$h_f = 2E+07v + 724.48 \quad (17)$$

$$k_f = 133.3v + 0.0044 \quad (18)$$

Table 3 summarizes the effect of feed flow rate on the heat transfer parameters. The increase in feed velocity (*Re*) resulted in the enhancement of *U* due to reduced feed film thickness at the liquid-vapor interface and related heat transfer resistances. Further, this enhancement in heat transfers with elevating *Re* number yields an increase in T_{fm} and thus reduce the temperature polarization effect. Consequently, the permeate flux increases.

c. Effect of vacuum pressure in permeate side

The increasing of vacuum pressure of the membrane downstream side at constant feed temperature and feed velocity, namely 338K and 0.00177 m s^{-1} respectively is investigated. Figs. 12 and 13 demonstrate that the heat and mass transfer coefficients in the liquid boundary interface are almost constant with decreasing the absolute pressure. VMD is characterized by vaporization at the membrane interface with the simultaneous diffusion of vapors through the membrane pores, which is usually

Table 3
Effect of feed velocity on the heat transfer parameters

v, m/s	*Q*, W/m²	*U*, W/m²·K	Re, ρuL/μ	Pr, cpμ/λ	*Nu*, h_fL/k	*Sc*, μ/ρD	*Sh*, k_fL/D
0.0010	21723	869	324.26	2.77	187.80	0.022	30.72
0.0014	24130	965	445.86	2.77	208.61	0.022	36.03
0.0018	26129	1045	567.46	2.77	225.89	0.022	40.64
0.0020	27306	1092	648.53	2.77	236.07	0.022	43.45
0.0022	28388	1136	729.59	2.77	245.43	0.022	46.08
0.0028	30332	1213	891.72	2.77	262.23	0.022	50.95
0.0030	31215	1249	972.79	2.77	269.87	0.022	53.21
0.0035	32844	1314	1134.9	2.77	283.95	0.022	57.48

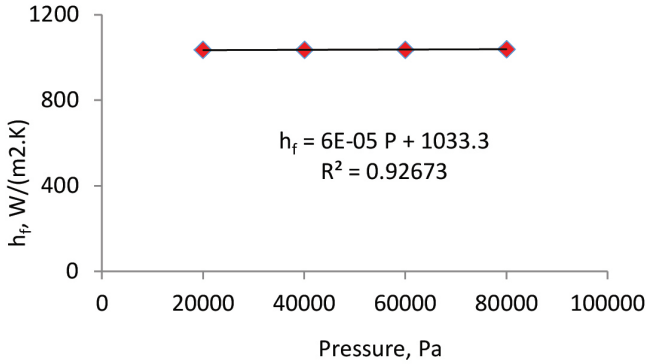

Fig. 12. Change of heat transfer coefficient of feed boundary layer with absolute pressure in the system.

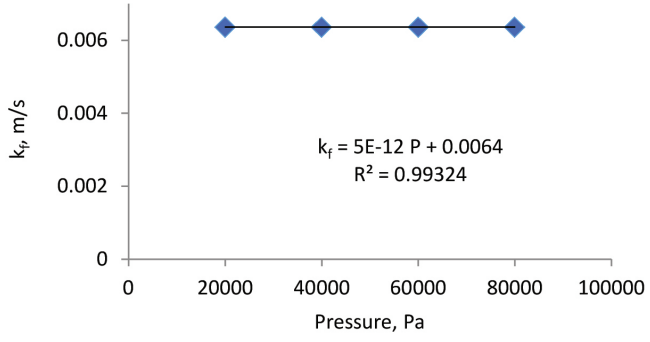

Fig. 13. Change of mass transfer coefficient of feed boundary layer with absolute pressure in the system.

based on the Knudsen mechanism [20]. At constant feed velocity and temperature, the temperature drop across the feed side boundary layer is almost constant irrespective of the vacuum pressure at the permeate side. Thus, the polarization factor, (θ), is reduced under elevated vacuum pressure resulting in negligible resistance in the liquid phase and the system is restricted to mass transfer across the membrane.

The following simplified equations of heat and mass transfer coefficients are formulated by linear regression.

$$h_f = (6E-05)\,P + 1033.3 \quad (19)$$

$$k_f = (5E-12)\,P + 0.0064 \quad (20)$$

Table 4 depicts the dependence of vacuum pressure changes on heat transfer parameters, where no noticeable changes occur in all parameters with the reduction in absolute pressure.

4.2. Experiments on saline water

Previous investigators concluded that the permeate flux decreases with increasing feed concentration, about 12% reduction in permeate flux occurred when the feed (NaCl) increased from 0 to 2 molar concentration [1,20,21]. The effect of salt concentration in the feed water, ranging from 3 to 40 kg m^{-3} Na Cl solutions, on heat and mass transfer parameters was investigated at constant feed flow rate (0.000014 $m^3\,s^{-1}$), absolute pressure (20000 Pa) and temperature (338K). The results show a significant fall in the heat and mass transfer coefficients when feed concentration is increased as illustrated in Figs. 14 and 15, respectively, mainly due to temperature and concentration

Table 4
Effect of absolute pressure on heat transfer parameters

Abs., P, Pa	*Q*, W/m²	*U*, W/m²·K	Re, ρuL/μ	Pr, cpμ/λ	*Nu*, h_fL/k	*Sc*, μ/ρD	*Sh*, k_fL/D
80000	25962	1038	514.94	3.089	226.90	0.024	45.18
60000	25915	1037	494.59	3.227	227.16	0.025	45.18
40000	25881	1035	484.18	3.315	227.56	0.026	45.18
20000	25872	1035	477.74	3.372	227.83	0.026	45.18

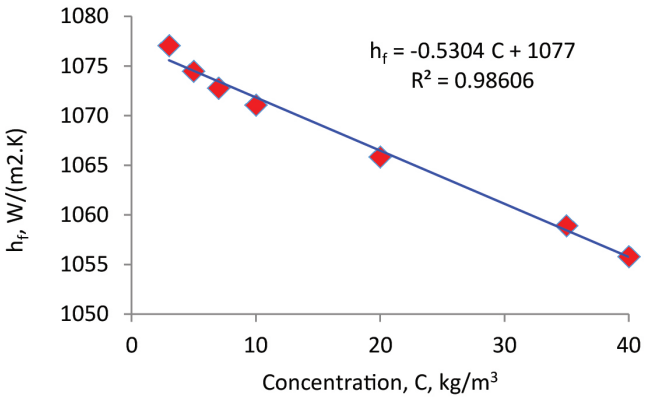

Fig. 14. Change of heat transfer coefficient of feed boundary layer with salt concentration at feed temperature 338 K, velocity 0.00177 m s^{-1} and 20000 Pa absolute pressure.

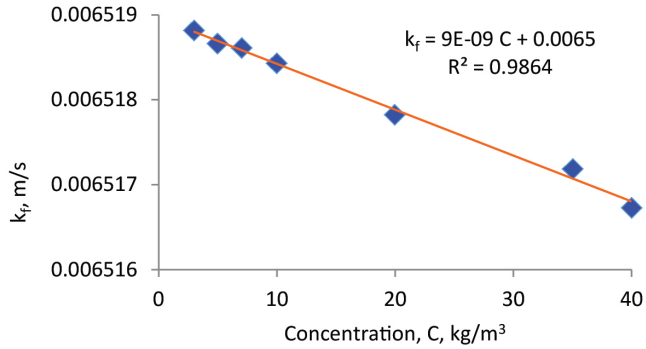

Fig. 15. Change of mass transfer coefficient of feed boundary layer with salt concentration at feed temperature 338 K, velocity 0.00177 m s^{-1} and 20000 Pa absolute pressure.

polarization effects. By increasing the feed concentration, the vapor pressure is reduced [22,23] and therefore, the temperature at the membrane interface, (T_{fm}), is decreased accompanied by an increase in (θ). On the other hand, the high salinity has high solution viscosity, which affects negatively the permeation of water molecules in the boundary membrane layer, i.e., increase the concentration polarization. Consequently, the heat transfer process through the liquid film is the controlling step in the process influenced by the increase of the boundary layer thickness with salinity, which in turn increases the resistance to the heat transfer process.

Relations between heat and mass transfer coefficients with concentration changes can be expressed by linear regression as the following equations:

$$h_f = -0.5304\ C + 1077 \quad (21)$$

$$k_f = 9E-09\ C + 0.0065 \quad (22)$$

where C is the salt concentration.

The estimated values of the main parameters are depicted in Table 5. As expected, the results indicate that all dimensionless groups are insignificantly varied with increasing salinity, which is probably attributed to the slight dependence of water physical properties on the concentration within the operating range.

5. Empirical correlations of heat and mass transfer coefficients

Generally, in the MD, the heat transfer coefficient of the boundary films is typically evaluated from known heat transfer empirical correlations acquired, and thus, merely usable for non-porous and rigid surfaces, which is completely opposite to the membrane surface. This contradiction may exhibit a difference in the heat transfer mechanism in MD systems and those for which the correlation equations were settled. Therefore, to overcome this lack, empirical correlations for simultaneous heat and mass transfer process in VMD is developed on the basis of the foregoing tests and results.

5.1. Empirical correlation for heat transfer boundary layer coefficient

The previous discussion, which is concerning the study of the effect of the operating parameters; feed temperature (T), absolute system pressure (P), feed velocity (v) and feed water salinity (C) on the transfer coefficients, reveals that these coefficients are directly proportional to the operating parameters, as depicted in the correlations that have been obtained by plotting the experimental transfer coefficients

Table 5
Effect of feed concentration on heat transfer parameters

C, kg/m³	Q, W/m²	U, W/m²·K	Re, ρuL/μ	Pr, cpμ/λ	Nu, h_fL/k	Sc, μ/ρD	Sh, k_fL/D
3	64284	2571	279.13	5.73	232.80	0.045	46.28
5	61245	2450	276.41	5.79	232.94	0.045	46.28
7	59219	2369	275.31	5.80	232.75	0.046	46.28
10	57064	2281	275.03	5.80	232.63	0.046	46.28
20	48571	1943	273.51	5.88	233.21	0.046	46.28
35	47119	1885	272.41	5.78	232.41	0.046	46.29
40	46669	1867	271.97	5.74	231.73	0.046	46.29

against the studied parameters. The plotting of the transfer coefficients versus the products of $T*P*v*C$ (the product of all influencing parameters affecting the mass and heat coefficients) gives linear and non-linear empirical formulae correlating the effect of all operating parameters on these coefficients. Fig. 16 depicts that the heat transfer coefficient is linearly correlated with $(T*P*v*C)$ for tap water experiments (estimated TDS is 0.7 kg m^{-3}), as well as for saline water within the experimental range studied. It is obvious from Fig. 16 that the increase of the product of the influencing parameters $(T*P*v*C)$ increasing the mass and heat transfer, due to the negligible effects of salt concentrations, while, it has a negative effect on these coefficients by increasing the feed salt concentration due to the effect of concentration polarization which has an impact on the transfer coefficients.

The experimental results may thus be conveniently represented by the following expressions [R^2 = 0.9677 and 0.9901]:

For fresh water:

$$h_f = 0.0489\ (T*P*v*C) + 751.64 \quad (23)$$

For saline water:

$$h_f = -4\text{E-}05\ (T*P*v*C) + 1077.2 \quad (24)$$

where T in K, P in Pa, v in ms^{-1} and C in kg m^{-3}.

The experimental heat transfer coefficient is plotted versus the calculated from the deduced Eqs. (23) and (24) (Fig. 17). It shows a fair correspondence between them with an error of ±3.7, which is calculated using sigma residual square technique, (SRS) (√(∑error^2) for N readings).

5.2. Empirical correlation for mass transfer coefficient

The same behavior of correlating the heat transfer coefficient in the liquid-membrane film is also adopted here for the correlation of mass transfer of vapor through the membrane (Fig. 18).

The following empirical formulae are obtained for estimating the mass transfer coefficient:

For fresh water:

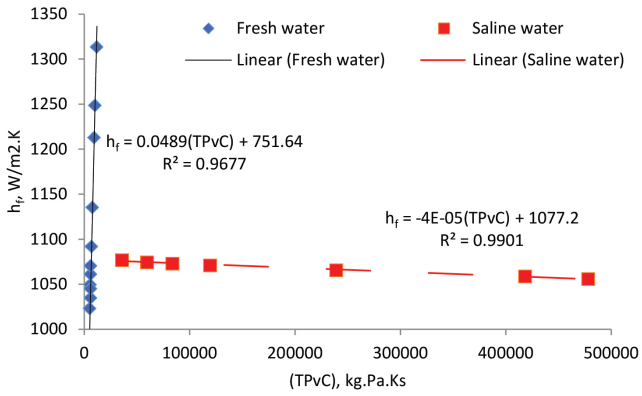

Fig. 16. Correlation of heat transfer boundary coefficients data.

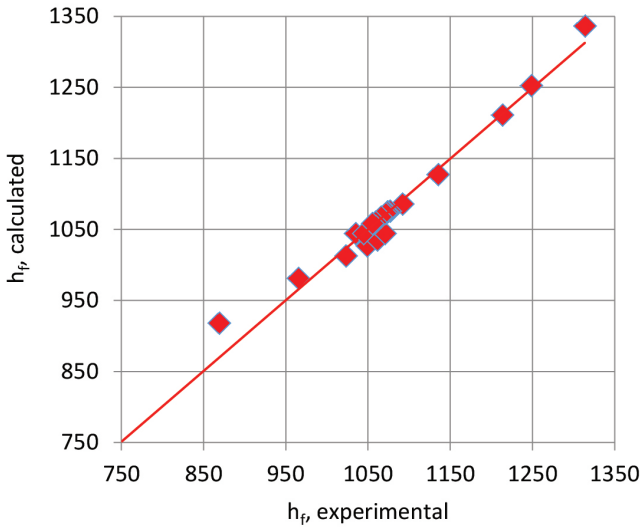

Fig. 17. Comparison between experimental and calculated heat transfer coefficient.

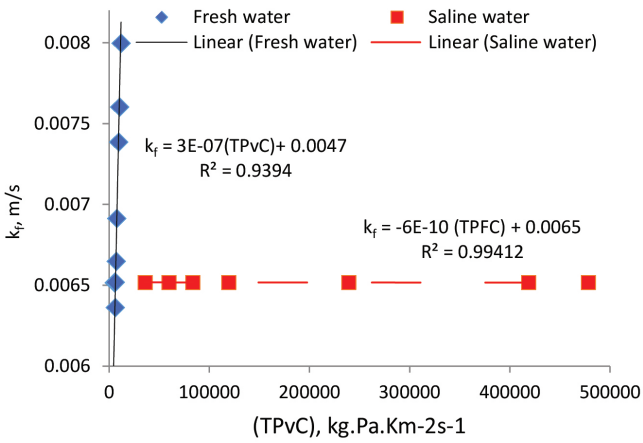

Fig. 18. Correlation of mass transfer coefficients data.

$$k_f = 3\text{E}{-}07\ (T*P*v*C) + 0.0047 \quad (25)$$

For saline water:

$$k_f = -6\text{E-}10\ (T*P*v*C) + 0.0065 \quad (26)$$

The experimental mass transfer coefficient is plotted versus the calculated from the deduced Eqs. (25), (26) as illustrated in Fig. 19. It shows a fair correspondence between them with an error of ±0.0003, which is calculated using the sigma residual square technique, (SRS) (√(∑error^2) for N readings).

6. Application of dimensionless analysis to mass transfer

The dimensionless group, denoted by Sherwood number, represents the mass transfer equivalent to the

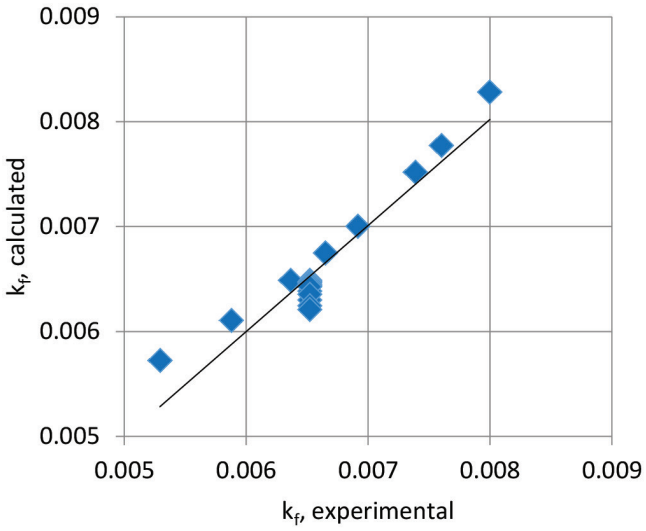

Fig. 19. Comparison between experimental and calculated mass transfer coefficients.

Nusselt number in heat transfer, with Prandtl number replaced by Schmidt number, via:

$$Sh = \text{constant } Re^a Sc^b \quad (27)$$

where the constants a and b are determined experimentally and iteratively to be 0.5 and 0.6 respectively. The exponent value corresponding to *Re* is as that earlier reported for mass transfer across cylinder in cross flow and for single sphere [24], but the exponent for *Sc* is rather higher than the one-third exponent previously stated. The difference in exponents depends on the hydrodynamic conditions and may have fundamental significance, since the transfer to a membrane surface, which can have ripples and tortuosity, should differ to a certain extent from transfer to a smooth rigid surface.

An empirical equation for the mass transfer in laminar flow representing the VMD system is thus proposed as derived from experimental data (Fig. 20) in the following:

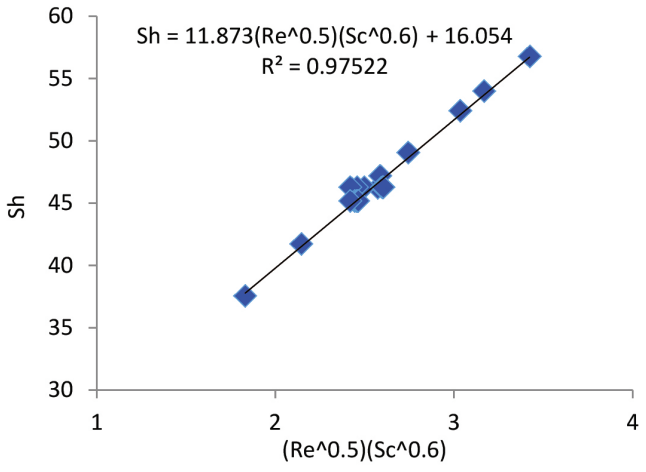

Fig. 20. Empirical correlation for Sherwood number.

$$Sh = 11.873\, Re^{0.5}\, Sc^{0.6} + 16.054 \quad (28)$$

The constant value of 16.054 may be attributed to natural convection developed within the liquid phase, which may be owing to the variation in the density resulting from relatively large concentration differences between the liquid and vapor.

6. Conclusions

The dependence of operating conditions of VMD process, for water purification and desalination of salt water in a previously prepared and tested flat (PES/TEOS) membrane module, on the mass and heat transfer coefficient investigated experimentally as well as theoretically. Consequently, the systematic study delivered valuable data for operation of a VMD for desalination; as how to maximize flux and heat transfer efficiency of the system. The results show that:

1. The impact of the heat and mass transfer resistances on the transport mechanism is significant and affects the water flux.
2. Increase in h_f and subsequently in k_f is strongly dependent on increasing the feed temperature (T), and the feed velocity (v) for the fresh water system, mainly due to a reduction in temperature polarization effect.
3. While, for saline water, the two above transport coefficients decrease with increasing the feed solution concentration, probably caused by the lowering of water vapor pressure and heat capacity owing to the presence of salt, which in turn produce a decrease in the driving force.
4. The experimental heat and mass transfer coefficients at the liquid-vapor interface is expressed as a linear function in T, P, v and C. The developed empirical correlations proved its capability in predicting the VMD transport coefficients, and it is, also, used in the calculation of the process performance.
5. An empirical correlation for Sherwood number for laminar flow is presented as a recommended equation to predict the mass transfer coefficient at the liquid-vapor interface in membrane distillation.

Acknowledgment

Authors would like to express their gratitude to "Science and Technology Development Fund" (STDF), Ministry of Scientific Research, Egypt, for funding the project entitled "Innovative Technology for Efficient and Cost-Effective Desalination by Membrane Distillation (MD)", Project ID: 552, Project Type: STDF – Water Desalination.

Symbols

C — Brine concentration, mol/m^3
C_p — Specific heat, J kg^{-1} K^{-1}
D — Diffusion coefficient (m^2 s^{-1})

d — Hydraulic diameter, m
h_f — Heat transfer coefficient in feed boundary layer, W m^{-2} K^{-1}
h_m — Heat transfer coefficient of the membrane layer (by conduction), W m^{-2} K^{-1}
h_p — Heat transfer coefficient of the permeate boundary layer, W m^{-2} K^{-1}
ΔHv — Heat of vaporization, W·s
J_{H_2O} — Molar flux of water, mol m^{-2} s^{-1}
k_f — Mass transfer coefficient of feed boundary layer, m s^{-1}, m·kg mol^{-1} s^{-1}
k_K — Membrane coefficient, mol·s kg^{-1} m^{-1}
k_m — Knudsen permeability, s mol$^{1/2}$ m^{-1} kg$^{-1/2}$
k_m — Thermal conductivity, W m^{-1} K^{-1}
M_{H_2O} — Molar mass of water, kg mol^{-1}
Nu — Nusselt number, dimensionless
P_m^* — Vapor pressure of pure water at membrane equilibrium conditions, Pa
P_p — Vapor pressure of water in the permeate side, Pa
ΔP_{H_2O} — Difference in partial pressure of water vapor on both sides of the membrane, Pa
Pr — Prandtl number (Eq. (12))
Q — Heat flux, w m^{-2}
R — The universal gas constant, kg m^2 s^{-2} K^{-1} mol^{-1}
r — Pore radius, m
Sc — Schmitt number (Eq. (11))
T_m — The temperature at the membrane surface, K
T — Temperature, K
T_f — Feed temperature, K
T_{fm} — Temperature on membrane surface at equilibrium, in the feed side, K
T_{pm} — Temperature on membrane permeate side at equilibrium, K
T_{ref} — Reference temperature, 20°C
U — Overall heat transfer coefficient, W m^{-2}·K^{-1}
v — velocity, m s^{-1}
v_f — Feed velocity, m s^{-1}
α — Slope
δ — Membrane thickness, m
ε — Membrane porosity
θ — Temperature polarization factor = $(T_f - T_{fm})/(T_f - T_V)$
χ — Tortuosity
μ — Viscosity, kg s^{-1} m^{-1}
ρ — Density of water, mol m^{-3}

References

[1] A. Alkhudhiri, N. Darwish, N. Hilal, Membrane distillation: A comprehensive review, Desalination, 287 (2012) 2–18.
[2] J.I. Mengual, L. Pena, Membrane distillation, Colloid Surf. Sc., 124 (1997) 17–29.
[3] C.R. Martinetti, A.E. Childress, T.Y. Cath, High recovery of concentrated RO brines using forward osmosis and membrane distillation, J. Membr. Sci., 331 (2009) 31–39.
[4] B. Li, K.K. Sirkar, Novel membrane and device for vacuum membrane distillation–based desalination process, J. Membr. Sci., 257 (2005) 60–75.
[5] T.D. Dao, J.P. Mericq, S. Laborie, C. Cabassud, A new method for permeability measurement of hydrophobic membranes in vacuum membrane distillation process, Water Res., 47 (2013) 2096–2104.
[6] H. Abdallah, A. El–Gendi, M. Khedr, E. ElZanati, Hydrophobic polyethersulfone porous membranes for membrane distillation, Front. Chem. Sci. Eng., 9(1) (2015) 84–93.
[7] B.L. Pangarkar, M.G. Sane, S.B. Parjane, R.M. Abhang, M. Guddad, The heat and mass transfer phenomena in vacuum membrane distillation for desalination, Int. J. Chem. Molec. Eng., 4(1) (2010) 69–74.
[8] M. Qtaishat, T. Matsuura, B. Kruczek M. Khayet, Heat and mass transfer analysis in direct contact membrane distillation, Desalination, 219(1–3) (2008) 272–292.
[9] M. Khayet, Membranes and theoretical modeling of membrane distillation: A review, Adv. Colloid Interface Sci., 164(1–2) (2011) 56–88.
[10] J.I. Mengual, M. Khayet, M.P. Godino, Heat and mass transfer in vacuum membrane distillation, Int. J. Heat Mass Transfer, 47 (2004) 865–875.
[11] M. Gryta, Effectiveness of water desalination by membrane distillation process, Membranes, 2 (2012) 415–429.
[12] M.A. Izquierdo-Gil, C. Fernández-Pineda, M.G. Lorenz, Flow rate influence on direct contact membrane distillation experiments: different empirical correlations for Nusselt number, J. Membr. Sci., 321(2) (2008) 356–363.
[13] M. Khayet, P. Godino, J.I. Mengual, Nature of flow on sweeping gas membrane distillation, J. Membr., Sci., 170(2) (2000) 243–255.
[14] N. Lior, A.M. Alklaibi, Membrane–distillation desalination: status and potential, Desalination, 171 (2005) 111–131.
[15] S. Gunko, S. Verbych, M. Bryk, N. Hilal, Concentration of apple juice using direct contact membrane distillation, Desalination, 190(1–3) (2006) 117–124.
[16] M.C. García-Payo, M.A. Izquierdo-Gil, C. Fernández-Pineda, Air gap membrane distillation of aqueous alcohol solutions, J. Membr. Sci., 169(1) (2000) 61–80.
[17] P. Termpiyakul, R. Jiraratananon, S. Srisurichan, Heat and mass transfer characteristics of a direct contact membrane distillation process for desalination, Desalination, 177 (2005) 133–141.
[18] E. El Zanati, Innovative Technology for Efficient and Cost–Effective Desalination by Membrane Distillation (MD), Project ID: 552, Project Type: STDF Water desalination, funded by Science and Technology Development Fund (STDF), Ministry of Scientific Research Ministry, Egypt., (2014).
[19] T.C. Chen, C.D. Ho, H.M. Yeh, Theoretical modeling and experimental analysis of direct contact membrane distillation, J. Membr. Sci., 330(1–2) (2009) 279–287.
[20] J. Xu, M. Furuswa, A. Ito, Air-sweep vacuum membrane distillation using fine silicone rubber, hollow fiber membranes, Desalination, 191 (2006) 223–231.
[21] M.A. Izquierdo-Gil, M.C. García-Payo, C. Fernández-Pineda, Air gap membrane distillation of sucrose aqueous solutions, J. Membr. Sci., 155(2) (1999) 291–307.
[22] F.A. Banat, J. Simandl, Theoretical and experimental study in membrane distillation, Desalination, 95 (1994) 39–52.
[23] L. Martínez, Comparison of membrane distillation performance using different feeds, Desalination, 168 (2004) 359–365.
[24] W.E. Ranz, W.R. Marshall, Evaporation from drops, Chem. Eng. Progr., 48(141–146) (1952) 173–180.